

# Diffuse LINER-type emission from extended disc regions of barred galaxies

S. M. Percival\* & P. A. James

*Astrophysics Research Institute, Liverpool John Moores University, IC2, Liverpool Science Park, 146 Brownlow Hill, Liverpool L3 5RF, UK*

Accepted 2020 May 13. Received 2020 May 13; in original form 2019 August 15

## ABSTRACT

We present a spectroscopic analysis of the central disc regions of barred spiral galaxies, concentrating on the region that is swept by the bar but not including the bar itself (the ‘Star Formation Desert’ or SFD region). New spectroscopy is presented for 34 galaxies, and the full sample analysed comprises 48 SBa - SBcd galaxies. These data confirm the full suppression of star formation within the SFD regions of all but the latest type (SBcd) galaxies. However, diffuse [NII] and H $\alpha$  line emission *is* detected in all galaxies. The ubiquity and homogeneous properties of this emission from SBa - SBc galaxies favour post-Asymptotic Giant Branch (p-AGB) stars as the source of this line excitation, rather than extreme Blue Horizontal Branch stars. The emission-line ratios strongly exclude any contribution from recent star formation, but are fully consistent with recent population synthesis modelling of p-AGB emission by other authors, and favour excitation dominated by ambient gas of approximately solar abundance, rather than ejecta from the AGB stars themselves. The line equivalent widths are also larger than those observed in many fully passive (e.g. elliptical) galaxies, which may also be a consequence of a greater ambient gas density in the SFD regions.

**Key words:** Galaxies : active - galaxies : spiral - galaxies : stellar content - galaxies : structure

## 1 INTRODUCTION

The presence of a bar in the centre of a disc galaxy has profound consequences for the evolution of that galaxy, with effects including the redistribution of gas, triggering, redistribution and quenching of star formation (SF), and the development of long-lived stellar components not seen in unbarred galaxies (Friedli & Benz 1993; Kormendy et al. 2004; Kormendy 2013). The timescales and interplay of these various gas-phase and stellar processes have yet to be determined in detail, however. In a series of papers, we have been looking at one specific mode of SF quenching that is intimately associated with strong bars in high-mass spiral galaxies. This was first seen through the discovery of strong suppression of H $\alpha$  line emission in some of the galaxies studied in the H $\alpha$  Galaxy Survey (H $\alpha$ GS; James et al. 2004), with the suppression being limited to the region of the disc ‘swept’ by a strong bar (James et al. 2009). The resulting ‘Star Formation Desert’ (SFD) as we termed it has significant global consequences for the galaxies concerned, as the affected area (a radial range extending approximately 1–5 kpc from the nucleus) is just the region that dominates

disc SF in unbarred galaxies. Thus this represents bars at least redistributing, and possibly suppressing, a significant fraction of the total SF in each affected galaxy.

In James & Percival (2015) we presented the first spectroscopic study of SFD regions, using long-slit optical spectra of 15 nearby barred galaxies to confirm that SFD regions are indeed devoid of SF activity (although nuclei at the bar centres and rings around the peripheries of bars are frequently host to vigorous SF). However, we found that SFD regions often contain diffuse low-surface-brightness line emission, with line ratios showing excitation that is clearly inconsistent with that expected from young stars. The extent of this emission, generally filling the SFD regions, argues against Active Galactic Nuclei (AGN) as the origin of the excitation, and our preferred explanation was instead the hard radiation field expected to result from post-Asymptotic Giant Branch (p-AGB) stars (Caldwell 1984; Phillips et al. 1986; Goudfrooij 1999; Graves et al. 2007; Singh et al. 2013; Bremer et al. 2013). For at least one galaxy in our study, this diffuse extended line emission shares fully in the rotational velocity of the disc of its host galaxy, supporting a link with the stellar component rather than an extended halo.

In subsequent papers (James & Percival 2016, 2018) we analysed absorption-line spectroscopy of SFD regions to de-

\* E-mail: S.M.Percival@ljmu.ac.uk

termine stellar population ages and metallicities. However, in the present paper, we return to the emission-line properties of these regions, using new data which extend the sample size from 15 galaxies in James & Percival (2015) to 48 galaxies, and improve the spectroscopic coverage of some of the galaxies already observed. With this improved dataset, we can explore further the ubiquity of the SFD phenomenon in barred galaxies, determine how common is the association of low-level diffuse line emission with these regions, and test the idea that that such emission is powered by p-AGB stars against other possibilities, such as bar-driven shocks or diffuse ionized gas (DIG) excited by leakage of ionizing photons from HII regions (Haffner et al. 2009). Other questions include the mechanism of the SF suppression; is this due to the efficient removal of gas from SFD regions, or is the gas still present but stabilised, e.g. by turbulent velocities generated by the bars?

### 1.1 Modelling line emission from evolved stellar populations

There is an extensive literature on both observational and theoretical studies of stellar-driven line emission that is not driven by star formation. A central question concerns the stellar evolutionary phase of the stars that dominate this emission, with the main candidates being p-AGB stars and Extreme Blue Horizontal Branch (EHB) stars. Here we briefly introduce some of the main studies that are relevant for the present analysis.

In an early study, Binette et al. (1994) demonstrated that p-AGB stars provide sufficient ionising radiation to account for the small but detectable H $\alpha$  luminosities and equivalent widths observed in some early-type galaxies. Stasińska et al. (2008) introduced the concept of ‘retired’ galaxies, i.e. those with no ongoing SF, and used population synthesis modelling to demonstrate that they can have detectable line emission due to p-AGB stars and hot white dwarfs, which may explain a substantial fraction of LINER-type galaxies, without recourse to AGN-driven excitation. Cid Fernandes et al. (2011) extended this analysis, and applied it to a large sample of galaxies for which spectroscopy of the central regions was available from the Sloan Digital Sky Survey (SDSS). They applied a diagnostic diagram using H $\alpha$  equivalent width (EW) and [NII]/H $\alpha$  line ratios to the classification of sources into star-forming, AGN, ‘retired’ and completely passive categories, finding a bimodal distribution in H $\alpha$  EW that distinguishes AGN from evolved star (assumed to be p-AGB) ionisation with a borderline at 3 Å; completely passive galaxies were found to have equivalent widths < 0.5 Å.

Belfiore et al. (2016) analysed data for 646 galaxies from the SDSS-IV MANGA survey, showing extended emission with LINER-type ratios in many of these. Again, they argued for p-AGB stars as the ionising source, and concluded that shock-excited galaxies are rare. Papaderos et al. (2013) and Gomes et al. (2016) presented a study of 32 early-type galaxies from the CALIFA survey, finding two classes of extended emission, both with LINER-type ratios. The classes are differentiated by their H $\alpha$  EW and radial profiles, with their type i group exhibiting stronger line emission (EW > 0.5Å) and steep radial gradients in this EW. This emission was attributed to p-AGB excitation, while the type

ii galaxies with low EW and shallower emission gradients were concluded to be dominated by ionizing photon leakage. Hirschmann et al. (2017) presented modelling of changes in emission line ratio as a function of cosmological epoch, and found p-AGB excitation to be important at lower redshifts, with AGN becoming more dominant at earlier cosmological epochs.

One study that is particularly relevant to the present paper is that of Byler et al. (2017, 2019), who have carried out probably the most comprehensive modelling of the emission-line properties of evolved stellar populations. Their analysis is based on MIST (Choi et al. 2016), which in turn builds on the MESA stellar synthesis models (Dotter 2016) plus the CLOUDY ionisation code (Ferland et al. 2013). Byler et al. (2019) find p-AGB emission to be ubiquitous in all but the very youngest populations; it is initiated at  $\sim 10^8$  years, and the continues until population ages of at least  $10^{10}$  years, with a slow decline in total ionising flux as a function of population age. However, as the population itself fades, the predicted H $\alpha$  EW actually rises slowly with age, in the range  $\sim 0.2 - 2.5$  Å. The use of CLOUDY enables them to predict line ratios from the gas around these p-AGB populations. If they assume ambient, pre-existing gas they find [NII]/H $\alpha$  line ratios that are clearly higher than those predicted for star-forming regions, but that lie in the intermediate range between star formation and the classic LINER-type regime, as defined by e.g. Kewley, Groves, Kauffmann & Heckman (2006). However, the models of Byler et al. (2017, 2019) do predict LINER-type ratios if they use what they call  $\alpha$ CN abundance ratios, such that the gas is enhanced in  $\alpha$  elements, carbon, and nitrogen, which they argue would be expected if the local environment of each p-AGB star is substantially enriched by gas lost by the star during its AGB evolution.

Another possible source of extended line emission is DIG, where the ionizing photons escape from HII regions, producing a low-surface-brightness floor of ionization on scales as large as kiloparsecs (Zurita et al. 2002; Zhang et al. 2017). Belfiore et al. (2016) find that this emission can have LINER-like emission line ratios, and Ferguson et al. (1996) claim that this extended component can comprise up to 50% of the H $\alpha$  emission, even in star-forming galaxies. Recent studies have confirmed this diffuse emission using deep Integral Field Unit observations; den Brok et al. (2020) study 41 galaxies with the MUSE instrument on the ESO Very Large Telescope, finding a diffuse H $\alpha$  fraction of  $\sim 30\%$  for one of the fitting methods they use, which they interpret as DIG. Weilbacher et al. (2018) also use MUSE in a study of the central regions and an outer tidal arm of ‘The Antennae’, NGC 4038/4039, again finding a diffuse component which they conclude can be excited by leakage of ionizing photons.

SFD regions provide a unique environment to test models of line emission powered by sources other than young stars, as they involve the central regions of gas-rich galaxies, but with no trace of the star formation which completely dominates such emission in most gas-rich galaxies. In this paper, we extend our earlier sample of 15 barred galaxies by adding deep long-slit spectroscopy for 34 systems. One of these had spectroscopy in our previous paper, and hence the combined dataset comprises 48 galaxies. Multiple slit position angles for several galaxies enable a comparison of the

line emission at additional positions within some of the SFD regions, and investigation of the spectroscopic appearance of bars themselves for comparison with their surrounding SFD regions.

The remainder of this paper is structured as follows. Section 2 contains a description of the galaxy sample, the new spectroscopic observations, and a brief account of the data reduction. The results of the spectroscopic analysis are given in Section 3, followed by a discussion of the consequences of these observations for our understanding of the SFD phenomenon in Section 4. Our conclusions are summarised in Section 5.

## 2 OBSERVATIONS

The 34 galaxies for which new spectroscopic data are presented here are listed in Table 1. The first 6 columns list the following galaxy properties: names, classifications, nuclear properties as listed in the NASA Extragalactic Database, recession velocities, adopted distances, and bar position angles in degrees anticlockwise from a North-South orientation. Columns 7 - 10 give some details of our observations: dates, integration times in seconds, slit position angles and the outer radius in kpc of the region extracted in our SFD spectroscopy. This sample supplements that presented in James & Percival (2015). Compared with our earlier study, the new sample is substantially larger, contains galaxies at broadly similar distances (mean 58.5 Mpc, range 14.1 – 122.8 Mpc, cf. a mean of 39.2 Mpc, range 10.2 – 95.5 Mpc for James & Percival 2015). The sample somewhat extends the Hubble-type range, in that we now have 6 early-types (SBa/SBab) cf. only one in the earlier study, and 5 late-types, classified SBcd, again cf. one previously.

The new observations presented here are long-slit optical spectra, taken with the Intermediate Dispersion Spectrograph (IDS) on the 2.5-metre Isaac Newton Telescope (INT) at the Roque de Los Muchachos Observatory on La Palma in the Canary Islands. The observing time was allocated to proposal I/2015A/07 by the UK Panel for the Allocation of Telescope Time. Observing dates allocated were 13 - 20/03/2015, but no data taken on last three nights due to poor weather. IDS was used with grating R1200Y, which has a blaze wavelength of 6000 Å. The detector used was Red+2, optimised for the longer optical wavelengths of primary interest here. The slit width used for all galaxy observations was 1.5'', giving a spectral dispersion corresponding to 0.53 Å/pixel and wavelength coverage of 1144 Å; the selected central wavelength was 6604 Å. The spatial pixel scale was 0.44''/pixel. We note that the slit position angles were set with respect to the bar axis, e.g. usually perpendicular to the bar for SFD observations, and so were *not* at the parallactic angle; however, atmospheric refraction effects are negligible for the [NII]/H $\alpha$  line ratios that are used here.

Flux calibration came from observations of spectrophotometric standard stars selected from the list at <http://catserver.ing.iac.es/landscape/tn065100/workflux.php>.

### 2.1 Data reduction

Data reduction of our long-slit spectroscopy was performed using Starlink software. All stages, i.e. bias subtraction, flat

fielding, correction of spectra for minor rotation and spatial distortion effects, sky background subtraction, wavelength calibration using a copper neon+ copper argon arc lamp and flux calibration from spectrophotometric standard observations were completely standard and will not be described further here. More details are given in James & Percival (2015), which also describes the use of H $\alpha$  narrow-band imaging to define the apparently emission-line free region from which the SFD spectra were extracted. In most cases, two SFD regions were extracted for each galaxy, one on either side of the nucleus (taking care to exclude all emission from the nuclear region).

The new analysis presented here resulted in 72 SFD spectra, from 34 galaxies, from which we were able to determine [NII]/H $\alpha$  emission line ratios for 66 of these regions (4 regions had no detected line emission, and 2 more showed H $\alpha$  but no [NII]). In combination with the 29 regions in 15 galaxies discussed in James & Percival (2015) and reanalysed here, this gives us a sample of 101 observed regions from a sample of 48 galaxies (noting that NGC 3185 was included in our earlier study and re-observed here), 93 of which have line detections enabling the calculation of line ratios. We also observed 6 galaxies with the slit aligned with the major axis of the bar, resulting in 11 off-nucleus bar regions with measured spectroscopic parameters to enable a preliminary comparison of bar and SFD properties.

As previously, at least one region of strong line emission from an HII region well outside the ‘desert’ was defined for all of the galaxies, to give reference line ratios corresponding to star formation. Line ratios were extracted for 59 such HII regions in the 48 galaxies of the extended sample.

This analysis resulted in line fluxes, line widths and central wavelengths for the H $\alpha$  6563 Å line, and the same parameters for the stronger of the two [NII] lines at 6584 Å plus equivalent widths for both lines.

## 3 RESULTS

### 3.1 Observed emission-line ratios

The upper frame in Fig. 1 shows the distribution of values of the observed [NII]6584 Å/H $\alpha$ 6563 Å line ratio (henceforth [NII]/H $\alpha$ ), for all of the SFD regions for which the two lines were detected. Ratios derived from SFD regions are shown as the solid histogram, while the corresponding values for the comparison HII regions are shown using dashed lines. The main histogram does not include line ratio data for the 5 late-type SBcd galaxies, however. While measurements were made for 9 regions in these galaxies, that are listed as ‘SFD’ in Table 2, all 9 show evidence for ongoing star formation, and hence in this plot we simply show their mean line ratio as a solid line in the upper-left hand corner of the plot, to demonstrate their consistency with the ratios found for HII regions (dashed histogram). As was found in James & Percival (2015), the latter form a very tight distribution around the values typical of excitation by star formation as found by numerous authors following the work of Baldwin, Phillips, & Terlevich (1981).

In the upper frame in Fig. 1, 17 regions are plotted in a single shaded histogram box to far right of the plot. These are regions which only had clear detections of the [NII] line,

**Table 1.** The galaxy sample and observational details for the new observations presented here. Position angles in italics are for observations along the axis of the bar.

Name	Class	Nucl(NED)	Vel km/s	Dist (Mpc)	Bar PA	Date obs	Int time	Slit PA	R <sub>MAX</sub> (kpc)
NGC1924	SB(r)bc		2558	36.0	45	20150315	3×1200	315	2.3
NGC2326	SB(rs)b		5985	90.4	130	20150317	3×1200	220	8.7
NGC2339	SAB(rs)bc	AGN	2206	33.0	70	20150313	3×1200	340	2.1
UGC3973	SBb	Sy1.2	6652	100.2	70	20150314	3×1200	340	4.5
UGC4042	(R)SB(r)b		8292	122.8	150	20150315	3×1200	60	6.2
NGC2487	SB(r)c		4841	71.9	45	20150314	3×1200	<i>43,315</i>	6.8
NGC2545	(R)SB(r)ab	LINER	3385	50.6	170	20150317	3×1200	260	1.7
NGC2523	SB(r)bc		3471	55.3	120	20150313	3×1200	60	7.1
NGC2604	SB(rs)cd	WR, HII, Sbrst	2078	32.7	50	20150316	(1)3×1200	<i>230,320</i>	2.8
NGC2746	SB(rs)a	AGN?	7065	105.6	40	20150315	3×1200	310	8.1
NGC3049	SB(rs)ab	HII, Sbrst	1455	24.2	35	20150316	3×1200	305	3.5
NGC3185	(R)SB(r)a	Sy2	1217	22.9	120	20150317	3×800	<i>30,285,300,315</i>	3.5
NGC3346	SB(rs)cd		1274	22.4	90	20150313	3×1200	0	1.2
UGC5892	SBb		8107	119.7	90	20150315	3×1200	180	3.3
NGC3374	SBc		7468	112.7	15	20150314	3×1200	285	4.1
NGC3485	SB(r)b:	AGN	1436	25.7	40	20150313	3×1200	130	1.8
NGC3507	SB(s)b	LINER	979	15.8	120	20150316	3×1200	30	2.0
NGC3729	SB(r)a pec		1060	20.2	20	20150315	3×1200	290	1.4
NGC3963	SAB(rs)bc		3188	51.5	130	20150314	3×1200	220	4.3
NGC4123	SB(r)c	WR, HII, Sbrst	1327	19.3	105	20150316	3×1200	15	2.5
NGC4416	SB(rs)cd	HII, Sbrst	1390	14.1	5	20150317	1×1200	95	0.6
NGC4619	SB(r)b	Sy1	6927	105.2	10	20150313	3×1200	100	3.2
NGC4779	SB(rs)bc	HII, Sbrst	2831	44.6	10	20150316	3×1200	100	3.9
NGC4904	SB(s)cd	HII, WR, Sbrst	1180	20.8	135	20150314	3(1)×1200	<i>45,315</i>	2.3
NGC4999	SB(r)b		5647	84.7	60	20150315	3×1200	330	8.5
NGC5164	SBb		7218	110.5	25	20150317	3×1200	115	3.8
NGC5350	SB(r)b	Sbrst	2321	39.3	110	20150313	3×1200	20	3.2
NGC5375	SB(r)ab		2386	39.9	170	20150316	3×1200	260	3.9
NGC5618	SB(rs)c		7132	106.7	5	20150317	3×1200	95	3.6
IC1010	SB(r)b pec		7702	115.3	170	20150315	3×1200	80	6.7
NGC5735	SB(rs)bc		3742	59.3	0	20150314	(1)3×1200	<i>0,270</i>	3.3
IC1067	SB(s)b		1577	27.5	140	20150313	3×1200	45	1.7
NGC5970	SB(r)c	HII, LINER	1957	28.4	80	20150315	(1,1,1)3×1200	<i>65,80,95,350</i>	1.8
NGC6004	SAB(rs)bc		3826	60.3	10	20150317	3×1200	100	2.3

and no H $\alpha$ , in the initial reduction of these spectra. However, these spectra still contain stellar absorption features, and in the next subsection we show that correction for absorption lines does reveal the presence of line emission in all of these cases.

### 3.2 Correction for underlying H $\alpha$ absorption

Measured H $\alpha$  emission-line fluxes will be reduced due to the presence of H $\alpha$  absorption features. In James & Percival (2015), we corrected for this by assuming that an absorption feature of the same equivalent width (EW) was present in all galaxy spectra. The EW value used was 1.103 Å, with an adopted uncertainty of 0.210 Å, within a bandpass of 8 Å. This corresponded to a simple stellar population (SSP) with a solar metallicity and an age of 3.5 Gyr, taken from the BaSTI population synthesis database (Percival et al. 2009). The BaSTI spectrum corresponding to this SSP was a reasonable ‘by-eye’ fit to the SFD spectra for the 15 galaxies discussed in James & Percival (2015).

However, a more sophisticated and self-consistent correction was needed for subsequent papers (James & Percival 2016, 2018), where the exact strength of the H $\beta$  absorp-

tion feature was needed, and infilling by H $\beta$  emission could strongly bias the stellar ages resulting from this measurement. Hence we adopted an iterative method enabling simultaneous fitting of emission and absorption features, which is described fully in James & Percival (2016). Briefly, this procedure starts by determining the strength of the H $\beta$  absorption feature by direct integration on the observed spectrum. This value is then used to identify the age of the best-fitting BaSTI SSP. The H $\alpha$  absorption EW is then taken from this model spectrum, and used to correct the H $\alpha$  emission line flux in the observed spectrum. This in turn is used to predict the H $\beta$  emission-line strength, using an H $\alpha$ /H $\beta$  flux ratio of 2.85 (Brocklehurst 1971; Hummer & Storey 1987). The initially-measured value of the H $\beta$  absorption is then corrected for the assumed presence of this emission line, and the corrected value is used to start the next stage of iterations.

In all cases, 3 or 4 cycles of iteration were sufficient to find a stable, self-consistent set of values for the H $\alpha$  and H $\beta$  emission and absorption line strengths. In James & Percival (2018), this process was applied to spectra of SFD regions in 21 galaxies, all of which are in the present study. A further 6 of the present sample have spectroscopy covering the

**Table 2.** The observed regions and extracted spectroscopic parameters for the full sample of 48 galaxies.

Name	Slit PA	Region	EW <sub>H<math>\alpha</math></sub>	err	EW <sub>[Nii]</sub>	err	[Nii]/H $\alpha$ (obs)	err	[Nii]/H $\alpha$ (cor)	err	Rad range "	Dir
NGC 1924	315	SFD1	2.42	0.14	2.51	0.24	1.038	0.111	0.668	0.108	3.1-6.2	NW
NGC 1924	315	SFD2	3.21	0.14	2.28	0.12	0.711	0.067	0.501	0.067	4.4-13.2	SE
NGC 1924	315	HII	50.52	0.25	20.15	0.20	0.399	0.011	0.389	0.011	16.7-22.4	SE
NGC 2326	220	SFD1	—	—	1.43	0.29	>1	—	1.068	0.228	5.7-19.8	SW
NGC 2326	220	SFD2	—	—	—	—	N/A	—	N/A	—	5.7-19.4	NE
NGC 2326	220	HII	7.84	0.47	3.27	0.26	0.417	0.100	0.356	0.096	20.7-25.1	SW
NGC 2339	340	SFD1	2.56	0.10	2.75	0.19	1.074	0.079	0.705	0.080	7.5-13.2	S
NGC 2339	340	SFD2	2.53	0.16	2.83	0.25	1.122	0.109	0.733	0.104	8.4-11.9	N
NGC 2339	340	HII	25.43	0.14	10.27	0.16	0.404	0.017	0.384	0.018	18.0-24.2	S
UGC 3973	340	SFD	1.26	0.18	2.58	0.29	2.050	0.179	0.993	0.140	7.0-9.2	SE
UGC 3973	340	HII	4.21	0.24	2.57	0.31	0.610	0.135	0.463	0.132	10.1-13.2	SE
UGC 4042	60	SFD1	1.68	0.20	1.62	0.18	0.965	0.163	0.536	0.136	3.3-10.4	NE
UGC 4042	60	SFD2	1.85	0.16	1.62	0.22	0.872	0.161	0.506	0.151	3.5-8.4	SW
UGC 4042	60	HII	25.28	0.32	10.53	0.27	0.416	0.028	0.395	0.028	9.2-11.9	SW
NGC 2487	315	SFD1	1.14	0.16	2.10	0.23	1.840	0.176	0.876	0.138	6.2-19.4	SE
NGC 2487	315	SFD2	—	—	1.32	0.14	>1	—	0.984	0.147	6.6-14.1	NW
NGC 2487	315	HII	16.03	0.22	6.31	0.25	0.394	0.042	0.363	0.043	22.4-29.0	SE
NGC 2487	43	Bar1	—	—	1.07	0.12	>1	—	0.801	0.150	6.2-16.7	SW
NGC 2487	43	Bar2	—	—	1.19	0.19	>1	—	0.891	0.190	6.2-17.2	NE
NGC 2487	43	HII	56.11	0.39	20.21	0.26	0.360	0.015	0.352	0.015	22.9-28.2	SW
NGC 2545	260	SFD1	1.23	0.11	1.59	0.13	1.296	0.121	0.620	0.107	3.1-6.2	W
NGC 2545	260	SFD2	1.10	0.10	1.25	0.10	1.135	0.124	0.512	0.108	3.1-7.0	E
NGC 2545	260	HII	13.44	0.15	5.50	0.16	0.410	0.031	0.372	0.032	7.1-10.6	W
NGC 2523	60	SFD1	—	—	0.34	0.04	>1	—	0.306	0.147	6.2-26.4	SW
NGC 2523	60	SFD2	—	—	—	—	N/A	—	N/A	—	6.2-21.6	NE
NGC 2523	60	HII	15.35	0.21	5.86	0.10	0.382	0.022	0.351	0.023	27.7-34.8	SW
NGC 2604	320	SFD1	8.23	0.31	2.27	0.21	0.276	0.101	0.237	0.100	7.9-13.2	NW
NGC 2604	320	SFD2	6.45	0.58	1.49	0.28	0.231	0.207	0.191	0.202	8.8-17.6	SE
NGC 2604	320	HII	42.82	0.69	8.40	0.33	0.196	0.042	0.190	0.042	15.0-19.4	NW
NGC 2604	230	Bar1	4.28	0.37	1.68	0.35	0.392	0.226	0.298	0.220	13.6-16.3	NE
NGC 2604	230	Bar2	25.23	0.38	6.96	0.25	0.276	0.039	0.262	0.039	11.9-15.0	SW
NGC 2604	230	HII	121.77	0.72	22.67	0.29	0.186	0.014	0.184	0.014	15.8-20.7	SW
NGC 2746	310	SFD1	1.44	0.10	0.75	0.17	0.523	0.234	0.271	0.232	4.4-15.8	NW
NGC 2746	310	SFD2	—	—	0.52	0.07	>1	—	0.385	0.167	5.5-11.7	SE
NGC 2746	310	HII	9.08	0.28	4.07	0.24	0.448	0.068	0.391	0.067	17.2-24.6	NW
NGC 3049	305	SFD1	12.65	0.86	7.51	0.67	0.594	0.112	0.537	0.109	12.8-16.3	NW
NGC 3049	305	SFD2	5.05	0.70	—	—	0.000	0.138	0.000	0.111	15.8-29.5	SE
NGC 3049	305	HII	34.33	0.73	9.91	0.58	0.289	0.063	0.278	0.063	17.6-21.1	NW
NGC 3185	300	Bar1	—	—	1.19	0.13	>1	—	0.886	0.147	7.04-25.1	NW
NGC 3185	300	Bar2	0.62	0.10	1.80	0.19	2.907	0.199	0.918	0.136	7.04-26.4	SE
NGC 3185	300	HII	18.97	0.38	7.29	0.25	0.385	0.040	0.359	0.040	33.4-37.8S	E
NGC 3185	30	SFD1	3.02	0.35	2.75	0.40	0.910	0.187	0.630	0.170	7.04-21.1	NE
NGC 3185	30	SFD2	1.73	0.22	3.04	0.36	1.754	0.175	0.989	0.146	7.04-19.8	SW
NGC 3185	30	HII	11.90	0.37	5.33	0.38	0.448	0.078	0.402	0.077	21.1-25.1	SW
NGC 3185	315	SFD3	1.43	0.17	1.96	0.30	1.371	0.195	0.708	0.172	7.04-31.7	NW
NGC 3185	315	SFD4	0.78	0.12	2.48	0.24	3.201	0.183	1.174	0.128	7.04-23.3	SE
NGC 3185	315	HII	28.98	0.53	11.06	0.30	0.381	0.033	0.365	0.033	36.1-40.5	SE
NGC 3185	285	SFD5	1.41	0.20	1.76	0.17	1.248	0.172	0.639	0.129	7.04-23.8	NW
NGC 3185	285	SFD6	1.14	0.15	2.16	0.16	1.888	0.148	0.870	0.109	7.04-24.6	SE
NGC 3185	285	HII	13.68	0.36	5.79	0.39	0.424	0.073	0.386	0.072	29.5-33.4	NW
NGC 3346	0	SFD1	2.60	0.16	1.94	0.21	0.748	0.123	0.502	0.119	6.6-10.6	N
NGC 3346	0	SFD2	2.61	0.21	1.68	0.18	0.645	0.132	0.450	0.123	5.3-11.4	S
NGC 3346	0	HII	29.37	0.23	9.09	0.19	0.309	0.022	0.296	0.023	16.3-23.3	S
UGC 5892	180	SFD1	2.51	0.23	1.87	0.18	0.747	0.131	0.487	0.117	3.5-5.7	S
UGC 5892	180	SFD2	2.40	0.10	2.00	0.22	0.836	0.118	0.536	0.119	3.5-5.7	N
UGC 5892	180	HII	25.81	0.28	11.48	0.30	0.445	0.029	0.423	0.029	6.6-9.2	N
NGC 3374	285	SFD1	3.79	0.24	3.62	0.27	0.956	0.098	0.706	0.093	3.9-6.6	ES
NGC 3374	285	SFD2	4.19	0.36	2.65	0.33	0.634	0.151	0.480	0.143	4.4-7.5	WN
NGC 3374	285	HII	42.72	0.35	12.64	0.26	0.296	0.022	0.287	0.022	14.1-20.2	ES

**Table 2** – *continued*

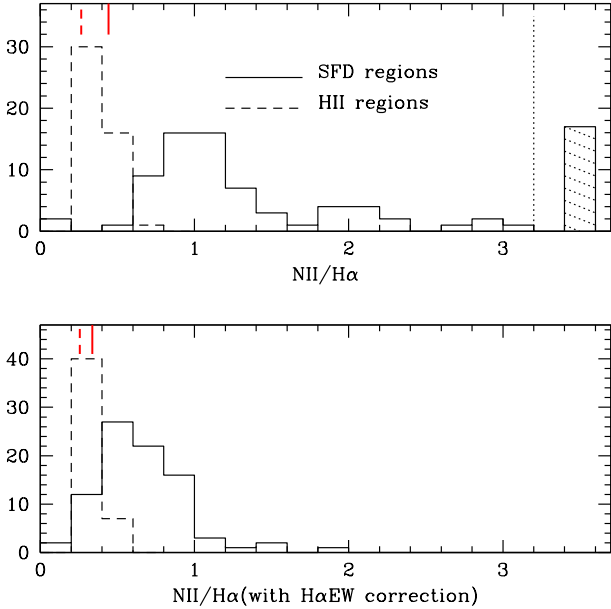
Name	Slit PA	Region	EW <sub>H<math>\alpha</math></sub>	err	EW <sub>[Nii]</sub>	err	[Nii]/H $\alpha$ (obs)	err	[Nii]/H $\alpha$ (cor)	err	Rad range "	Dir
NGC 3485	130	SFD1	—	—	1.08	0.16	>1	—	1.078	0.181	5.3-14.5	NW
NGC 3485	130	SFD2	—	—	0.94	0.10	>1	—	0.609	0.149	5.3-12.8	SE
NGC 3485	130	HII	48.79	0.33	16.26	0.24	0.333	0.016	0.324	0.016	24.6-30.0	NW
NGC 3507	30	SFD1	1.10	0.11	1.57	0.12	1.434	0.124	0.635	0.105	6.2-23.8	NE
NGC 3507	30	SFD2	0.94	0.09	1.31	0.09	1.389	0.112	0.563	0.096	6.2-26.4	SW
NGC 3507	30	HII	20.35	0.19	7.97	0.19	0.392	0.025	0.367	0.026	36.1-40.5	NE
NGC 3729	290	SFD1	4.42	0.13	4.70	0.19	1.062	0.050	0.820	0.051	4.4-14.1	NW
NGC 3729	290	SFD2	3.91	0.13	3.69	0.23	0.942	0.071	0.695	0.072	6.2-14.5	SE
NGC 3729	290	Clump	5.39	0.16	5.63	0.19	1.045	0.045	0.837	0.046	4.4-7.0	NW
NGC 3729	290	HII	29.38	0.12	9.77	0.14	0.332	0.015	0.318	0.016	17.2-22.4	SE
NGC 3963	220	SFD	2.00	0.19	1.62	0.16	0.810	0.138	0.485	0.123	5.7-17.2	SW
NGC 3963	220	HII	19.91	0.25	7.65	0.23	0.384	0.033	0.360	0.033	19.8-26.0	SW
NGC 4123	15	SFD1	4.72	0.39	3.80	0.27	0.805	0.110	0.612	0.099	8.8-26.4	N
NGC 4123	15	SFD2	3.13	0.37	3.70	0.44	1.182	0.166	0.828	0.147	8.8-23.3	S
NGC 4123	15	HII	32.75	0.99	10.08	0.64	0.308	0.071	0.296	0.070	42.7-46.2	N
NGC 4416	95	SFD1	10.69	0.25	3.36	0.16	0.315	0.053	0.280	0.053	4.4-8.8	E
NGC 4416	95	SFD2	11.04	0.23	4.16	0.22	0.377	0.056	0.336	0.057	4.4-8.8	W
NGC 4416	95	HII	23.40	0.46	6.88	0.47	0.294	0.071	0.278	0.071	22.9-26.8	W
NGC 4619	100	SFD1	2.01	0.06	2.03	0.12	1.009	0.067	0.606	0.074	2.6-6.2	E
NGC 4619	100	SFD2	2.05	0.12	1.97	0.16	0.958	0.099	0.580	0.096	2.6-5.3	W
NGC 4619	100	HII	14.35	0.12	6.46	0.17	0.450	0.028	0.412	0.029	7.0-11.0	W
NGC 4779	100	SFD1	3.83	0.30	2.99	0.16	0.781	0.096	0.569	0.084	5.3-13.6	E
NGC 4779	100	SFD2	2.45	0.20	2.08	0.14	0.849	0.104	0.558	0.091	5.3-18.0	W
NGC 4779	100	HII	193.95	0.83	58.55	0.30	0.302	0.007	0.300	0.007	20.2-24.6	W
NGC 4904	45	SFD1	3.90	0.19	1.96	0.10	0.502	0.070	0.373	0.067	11.4-22.4	NE
NGC 4904	45	HII	53.41	0.58	13.11	0.26	0.245	0.023	0.239	0.023	30.4-24.8	SW
NGC 4904	315	Bar1	9.36	0.26	3.59	0.16	0.384	0.051	0.336	0.051	19.4-21.6	NW
NGC 4904	315	HII	50.69	0.75	13.18	0.16	0.260	0.019	0.253	0.019	23.8-27.7	NW
NGC 4999	330	SFD1	1.45	0.08	1.47	0.16	1.012	0.122	0.520	0.121	6.2-16.3	NW
NGC 4999	330	SFD2	1.65	0.31	1.01	0.03	0.608	0.191	0.310	0.113	6.2-20.7	SE
NGC 4999	330	HII	10.88	0.18	3.12	0.14	0.287	0.048	0.255	0.048	22.4-26.4	SE
NGC 5164	115	SFD1	1.52	0.18	1.31	0.27	0.863	0.239	0.458	0.223	3.5-7.1	SE
NGC 5164	115	SFD2	—	—	—	—	N/A	—	N/A	—	3.5-6.6	NW
NGC 5164	115	HII	11.70	0.49	4.01	0.30	0.343	0.085	0.308	0.084	9.7-13/2	SE
NGC 5350	20	SFD1	0.80	0.13	1.12	0.14	1.402	0.207	0.534	0.156	6.2-13.6	N
NGC 5350	20	SFD2	—	—	1.57	0.15	>1	—	1.210	0.140	6.6-16.7	S
NGC 5350	20	HII	35.45	0.16	12.61	0.22	0.356	0.018	0.343	0.018	32.6-39.6	S
NGC 5375	260	SFD1	0.67	0.11	0.67	0.08	1.010	0.200	0.330	0.147	4.4-19.4	W
NGC 5375	260	SFD2	—	—	0.46	0.04	>1	—	0.310	0.129	4.4-20.2	E
NGC 5375	260	HII	6.46	0.23	3.11	0.26	0.481	0.090	0.399	0.090	22.9-30.3	W
NGC 5618	95	SFD1	1.65	0.34	—	—	0.000	0.208	0.000	0.123	3.5-7.0	E
NGC 5618	95	SFD2	1.30	0.31	0.96	0.21	0.741	0.329	0.364	0.257	3.5-6.6	W
NGC 5618	95	HII	8.34	0.26	4.94	0.45	0.592	0.095	0.510	0.095	12.8-16.3	W
IC 1010	80	SFD1	—	—	1.98	0.19	>1	—	1.472	0.140	4.8-11.9	E
IC 1010	80	SFD2	—	—	—	—	N/A	—	N/A	—	4.8-8.4	W
IC 1010	80	HII	14.65	0.41	7.06	0.45	0.482	0.070	0.441	0.069	13.2-17.2	W
NGC 5735	270	SFD1	1.30	0.16	1.17	0.15	0.904	0.178	0.445	0.149	6.6-11.4	N
NGC 5735	270	SFD2	0.88	0.13	2.04	0.21	2.307	0.182	0.917	0.133	5.3-11.0	S
NGC 5735	270	HII	14.70	0.33	5.50	0.20	0.374	0.043	0.343	0.043	22.4-27.3	S
NGC 5735	0	Bar1	1.56	0.20	1.90	0.21	1.222	0.171	0.657	0.140	3.1-6.2	W
NGC 5735	0	Bar2	2.36	0.09	1.50	0.14	0.634	0.101	0.404	0.103	2.6-6.1	E
NGC 5735	0	HII	22.51	0.19	7.73	0.18	0.343	0.025	0.324	0.026	10.1-14.1	E
IC 1067	45	SFD1	—	—	0.64	0.11	>1	—	0.481	0.195	3.9-12.8	NE
IC 1067	45	SFD2	—	—	0.55	0.12	>1	—	0.410	0.243	4.4-12.3	SW
IC 1067	45	HII	26.66	0.51	11.34	0.51	0.425	0.049	0.405	0.049	14.5-19.8	SW
NGC 5970	350	SFD1	0.81	0.07	1.23	0.08	1.521	0.108	0.539	0.095	4.4-8.8	N
NGC 5970	350	SFD2	1.20	0.05	1.42	0.07	1.181	0.063	0.497	0.078	4.4-9.7	S
NGC 5970	350	HII	74.01	1.04	28.35	0.44	0.383	0.021	0.376	0.021	15.4-20.2	N
NGC 5970	80	Bar1	0.84	0.13	1.12	0.08	1.338	0.172	0.515	0.111	3.1-7.5	E
NGC 5970	80	Bar2	1.78	0.08	1.29	0.05	0.724	0.059	0.413	0.063	3.9-12.8	W

Table 2 – *continued*

Name	Slit PA	Region	EW <sub>H<math>\alpha</math></sub>	err	EW <sub>[NII]</sub>	err	[NII]/H $\alpha$ (obs)	err	[NII]/H $\alpha$ (cor)	err	Rad range "	Dir
NGC 5970	80	HII	65.87	0.89	20.37	0.41	0.309	0.024	0.303	0.024	26.4-30.4	E
NGC 5970	65	SFD3	0.79	0.10	0.82	0.05	1.036	0.140	0.384	0.097	4.0-9.7	EN
NGC 5970	65	SFD4	1.03	0.14	0.92	0.06	0.897	0.149	0.389	0.102	4.0-8.4	WS
NGC 5970	65	HII	13.21	0.15	4.36	0.16	0.330	0.039	0.300	0.040	14.5-18.9	EN
NGC 5970	95	SFD5	1.63	0.14	1.02	0.08	0.630	0.114	0.345	0.099	3.5-8.4	E
NGC 5970	95	SFD6	2.09	0.13	1.29	0.06	0.616	0.079	0.376	0.072	2.6-7.0	W
NGC 5970	95	HII	20.52	0.14	5.15	0.11	0.251	0.023	0.236	0.024	15.4-9.8	E
NGC 6004	100	SFD	2.35	0.31	2.17	0.17	0.925	0.155	0.589	0.122	3.5-7.9	E
NGC 6004	100	HII	23.52	0.30	8.64	0.30	0.367	0.037	0.348	0.037	13.6-17.1	E
NGC 864	55	SFD1	—	—	0.88	0.16	>1	—	0.656	0.207	10.12-32.12	NE
NGC 864	55	SFD2	1.31	0.16	—	—	0.000	—	0.000	1.003	19.36-33.88	SW
NGC 864	55	HII	93.18	0.93	20.81	0.84	0.223	0.040	0.220	0.042	67.76-73.92	NE
NGC 2268	183	SFD1	1.94	0.12	2.46	0.16	1.267	0.069	0.750	0.085	3.08-4.84	N
NGC 2268	183	SFD2	2.81	0.09	2.85	0.13	1.017	0.047	0.687	0.060	3.96-7.04	S
NGC 2268	183	HII	72.14	1.03	25.32	0.51	0.351	0.020	0.345	0.025	8.36-11.44	S
UGC 3685	0	SFD1	0.83	0.15	1.72	0.28	2.076	0.195	0.942	0.190	7.48-17.60	N
UGC 3685	0	SFD2	1.60	0.13	1.44	0.21	0.895	0.152	0.510	0.159	7.48-17.60	S
UGC 3685	0	HII	48.09	0.69	13.63	0.45	0.283	0.033	0.276	0.036	30.80-36.08	S
NGC 2543	180	SFD1	1.19	0.21	1.17	0.31	0.983	0.296	0.402	0.281	7.48-24.20	N
NGC 2543	180	SFD2	1.67	0.20	1.88	0.37	1.125	0.211	0.557	0.212	6.60-19.80	S
NGC 2543	180	HII	86.41	1.73	26.75	0.77	0.310	0.029	0.305	0.035	23.32-26.40	S
NGC 2595	260	SFD1	—	—	—	—	NA	—	N/A	—	9.68-19.36	E
NGC 2595	260	SFD2	2.59	0.29	1.79	0.30	0.693	0.180	0.416	0.185	13.20-26.40	W
NGC 2595	260	HII	26.31	0.34	10.72	0.25	0.408	0.023	0.388	0.027	23.76-29.92	E
NGC 2712	350	SFD1	1.00	0.11	1.44	0.16	1.441	0.123	0.618	0.134	6.16-21.56	S
NGC 2712	350	SFD2	1.49	0.10	1.59	0.15	1.069	0.099	0.577	0.111	7.48-20.68	N
NGC 2712	350	HII	19.66	0.33	7.58	0.23	0.385	0.031	0.361	0.035	33.00-44.44	N
NGC 3185	320	SFD1	0.39	0.13	1.14	0.11	2.908	0.208	0.728	0.148	9.68-21.56	SE
NGC 3185	320	SFD2	0.45	0.11	0.84	0.12	1.862	0.203	0.552	0.175	11.44-29.04	NW
NGC 3185	320	HII	10.83	0.21	4.34	0.18	0.401	0.042	0.357	0.046	33.44-42.68	NW
NGC 3351	200	SFD1	—	—	1.95	0.42	>1	—	1.454	0.237	27.28-51.48	NNE
NGC 3351	200	SFD2	—	—	1.33	0.13	>1	—	0.992	0.140	25.52-40.92	SSW
NGC 3351	200	HII	16.37	0.40	4.99	0.35	0.305	0.071	0.282	0.074	73.48-58.08	NNE
NGC 3367	170	SFD1	2.39	0.17	3.03	0.07	1.271	0.028	0.848	0.062	5.28-9.68	N
NGC 3367	170	SFD2	4.76	0.36	5.27	0.29	1.107	0.061	0.898	0.085	5.72-10.12	S
NGC 3367	170	HII	46.25	0.58	13.55	0.25	0.293	0.019	0.285	0.022	11.88-16.28	N
NGC 3811	267	SFD1	1.13	0.11	1.07	0.13	0.950	0.131	0.426	0.140	5.28-10.56	W
NGC 3811	267	SFD2	0.35	0.10	1.24	0.13	3.581	0.186	0.750	0.144	5.28-10.56	E
NGC 3811	267	HII	103.17	2.43	33.05	0.92	0.320	0.028	0.316	0.036	21.56-24.64	W
NGC 4051	117	SFD	0.19	0.04	0.56	0.04	2.897	0.116	0.366	0.116	12.76-32.12	NW
NGC 4051	117	HII	34.88	0.92	11.49	0.35	0.329	0.031	0.317	0.040	71.28-81.84	NW
NGC 4210	170	SFD1	0.65	0.11	1.30	0.11	2.017	0.113	0.653	0.121	3.08-5.72	N
NGC 4210	170	SFD2	—	—	1.07	0.14	>1	—	0.798	0.165	3.52-6.16	S
NGC 4210	170	HII	15.99	0.08	6.15	0.20	0.385	0.033	0.355	0.034	11.00-15.40	N
NGC 5698	70	SFD1	1.05	0.25	1.93	0.24	1.831	0.181	0.852	0.175	6.16-22.00	WSW
NGC 5698	70	SFD2	—	—	2.64	0.20	>1	—	1.992	0.125	7.04-19.36	ENE
NGC 5698	70	HII	74.92	0.63	24.39	0.56	0.326	0.023	0.320	0.024	33.88-37.84	ENE
NGC 5806	30	SFD1	0.84	0.07	1.74	0.13	2.072	0.082	0.794	0.102	6.60-13.20	SW
NGC 5806	30	SFD2	0.60	0.09	1.65	0.12	2.744	0.095	0.892	0.111	6.60-11.44	NE
NGC 5806	30	HII	6.65	0.16	2.92	0.14	0.440	0.049	0.365	0.055	15.40-24.20	NE
UGC 10888	120	SFD1	0.89	0.16	2.08	0.38	2.332	0.215	0.933	0.205	3.96-9.24	NW
UGC 10888	120	SFD2	—	—	0.92	0.15	>1	—	0.686	0.191	3.96-8.80	SE
UGC 10888	120	HII	22.08	0.32	9.42	0.29	0.427	0.031	0.402	0.034	10.56-18.48	NW

H $\alpha$ , H $\beta$  and Mgb lines, enabling the implementation of this iterative method. For the remaining 21 galaxies, only red spectroscopy covering the H $\alpha$  and [NII] regions was available. For these, the H $\alpha$  fluxes have been corrected assuming a fixed absorption EW. However, the best-fit models for the iterative fits to spectra from the other 27 galaxies cor-

responded to SSPs with significantly younger ages, 1.9 Gyr rather than the 3.5 Gyr assumed in James & Percival (2015). This results in a correction with 1.34 Å EW, rather than the 1.103 Å EW used previously. The new value is applied to all of the spectra for which the iterative method cannot be used, and hence updated values of [NII]/H $\alpha$  are presented



**Figure 1.** Upper frame: Histogram of observed  $[\text{NII}]/\text{H}\alpha$  line ratios for SFD (solid line) and HII (dashed line) regions with data presented here. The  $\text{H}\alpha$  fluxes have no correction for underlying  $\text{H}\alpha$  absorption features. The points to the right of the dotted line correspond to regions detected in  $[\text{NII}]$  only. Only SFD regions observed with the slit perpendicular to the bar axis (‘SFD1’ and ‘SFD2’ in Table 2) are included. Lower frame: As for the upper frame, but after correction for underlying  $\text{H}\alpha$  absorption. The solid and dashed lines to the upper left show the mean line ratios for equivalent regions in 9 SFD regions within 5 late-type Scd spiral galaxies.

in Table 2 (below the horizontal line) for the spectroscopy already presented in James & Percival (2015). The updated corrections will be used for all line ratios and  $\text{H}\alpha$  EW values discussed in the remainder of this paper, for SFD, HII and bar regions.

### 3.3 Emission-line ratios and equivalent widths after absorption correction

The lower frame of Fig. 1 shows the effect on  $[\text{NII}]/\text{H}\alpha$  line ratios of boosting the  $\text{H}\alpha$  emission-line fluxes using either the iterative correction method or the  $1.34 \text{ \AA}$  equivalent width correction as explained above. The effect on ratios from HII regions is small, as expected given the high EW line emission. For the SFD regions, the absorption line correction significantly compresses the range of measured ratios, and removes the group of 17 regions for which only  $[\text{NII}]$  emission was detected. After application of the absorption correction, all are concluded to have  $\text{H}\alpha$  emission, at levels that make their line ratios consistent with the remainder of the population. More quantitatively, for the 87 SFD regions, after the application of absorption corrections and with the late-type Scd galaxies removed, the mean observed  $[\text{NII}]/\text{H}\alpha$  ratio is  $0.648 \pm 0.033$ , median 0.573. For the 53 HII regions in the same galaxies, the mean absorption-corrected  $[\text{NII}]/\text{H}\alpha$  ratio is  $0.347 \pm 0.008$ , median 0.355. A Kolmogorov-Smirnov test

applied to the distributions of SFD and HII region line ratios gives a maximum difference in the cumulative normalised distributions  $D = 0.7554$ , with a probability  $P = 0.000$  of their being drawn from the same parent distribution. Thus, while the strong absorption correction has closed up the distributions, the SFD region ratios are much too high to be consistent with SF.

The mean corrected line ratio for SFD regions in late-type Scd galaxies is now  $0.338 \pm 0.058$ , more consistent with the values for HII regions than for SFD regions of galaxies of other, earlier types. In these 5 galaxies only, the line emission in the SFD regions *does* seem to be dominated by SF. This confirms the suggestion by Nair & Abraham (2010) and Hakobyan et al. (2014) that bars in late-type disc galaxies have quite different effects on star formation properties from those with earlier-type hosts, and justifies our separating out these 5 galaxies from the remainder of the sample in our analysis of the SFD phenomenon in bar-swept regions.

We are now in a position to analyse  $\text{H}\alpha$  and  $[\text{NII}]$  EW values and line ratios for the SFD regions, with the  $\text{H}\alpha$  values having been corrected for absorption. The mean EW values are  $2.791 \pm 0.134 \text{ \AA}$  for  $\text{H}\alpha$ , and  $1.762 \pm 0.106 \text{ \AA}$  for  $[\text{NII}]$ . These means are somewhat higher than the predictions for fully passive galaxies from the models of Byler et al. (2017) and Byler et al. (2019), and than the observed EW values for the ‘retired galaxies’ of Cid Fernandes et al. (2011). Figure 2 shows the distribution of the SFD regions on a ‘WHAN’ diagram (Cid Fernandes et al. 2011) of  $\text{H}\alpha$  equivalent-width as a function of  $[\text{NII}]/\text{H}\alpha$  line ratio. Almost all of the SFD regions lie within the locus defined by Cid Fernandes et al. (2011) to correspond to LINER-type emission. A small number of regions have sufficiently strong emission lines that they cross into the Seyfert/AGN or star formation region; these include most of the galaxies that we identified above as being late-type galaxies with ongoing SF (open circles in Fig. 2). The arrows correspond to SFD spectra where  $\text{H}\alpha$  lines are measurable but no  $[\text{NII}]$  lines are seen. These results will be discussed further in Sect. 4.

### 3.4 Is this diffuse emission excited directly by bars?

One possible mechanism for exciting line emission with high  $[\text{NII}]/\text{H}\alpha$  ratios is through shocks (Baldwin, Phillips, & Terlevich 1981), given that the shock models of e.g. Allen et al. (2008) nicely reproduce the  $[\text{NII}]/\text{H}\alpha$  line ratios found here, and in SFD regions shocks could plausibly be driven by the bar itself. In order to test this possibility, we performed an analysis of two galaxies using multiple slit angles, to test whether emission peaks ‘downstream’ of bars. The two galaxies chosen were NGC 3185 and NGC 5970, types SBa and SBc respectively, both of which show ‘normal’ LINER-type emission in their SFD regions as measured perpendicular to the bar axis. Both were additionally observed with the slit position angle along the bar, at  $+15^\circ$  and  $-15^\circ$  to the bar major axis, and also at  $+20^\circ$  for NGC 3185 (positive angles are defined as increasing anticlockwise, which is the rotation direction deduced for both galaxies, assuming trailing spiral arms). The resulting values are listed in Table 2 as ‘SFD3’ - ‘SFD6’.

Figure 3 shows the negative results of this test, with no

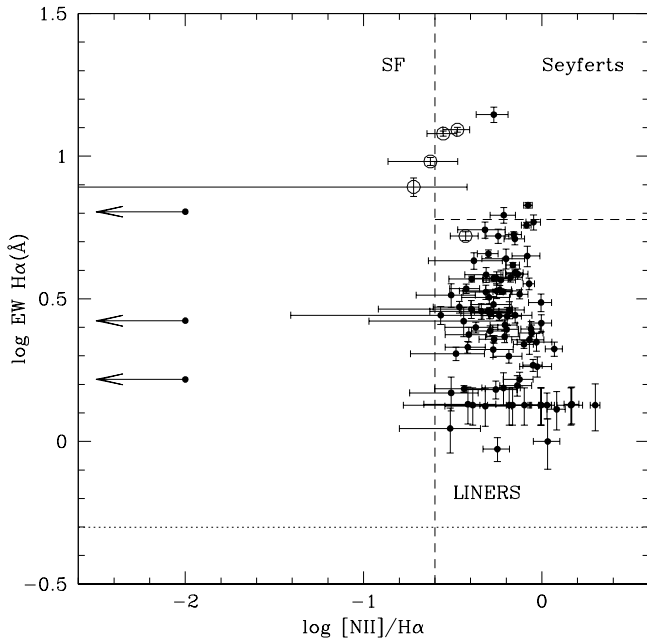


**Figure 2.** A ‘WHAN’ diagram (Cid Fernandes et al. 2011) showing  $H\alpha$  equivalent width as a function of  $[NII]/H\alpha$  line ratio, where the dashed lines mark the boundaries separating emission powered by star formation, Seyfert/AGN activity and LINER-type emission. The dotted line corresponds to an  $H\alpha$  equivalent width of  $0.5 \text{ \AA}$ , the upper limit proposed in the literature for emission from old populations in early-type galaxies.

systematic variation in  $[NII]$  emission line EW being found with changing slit position angle. For each angle, the point indicates the mean of the ratios observed on either side of the nucleus, and the ends of the error bars indicate the two individual values. The earlier-type NGC 3185 has higher line ratios at all positions, but neither galaxy shows a significant difference in line ratios around the bar, that might indicate an ‘upstream’ vs. ‘downstream’ variation, and the values measured close to the bar do not show any convincing difference compared to those measured perpendicular to the bar. Analysis of the  $[NII]/H\alpha$  line ratio (not shown) also shows no evidence for variation with position relative to the bar. We conclude that there is no evidence for bar-driven shock excitation of this emission. One consequence of this is that spectra taken with all slit orientations  $\geq 15^\circ$  from the bar axis can be considered representative of the SFD, and will be included as such in statistical statements about SFD properties in this paper. However, given that only two galaxies were included in this analysis, no strong general statements can be made about the possible contribution of shocks to the diffuse line emission in SFD regions. The  $[OI]6300\text{\AA}$  line, which gives stronger diagnostics of shock excitation, was not detected in any of the SFD regions.

### 3.5 Spectroscopic comparison of bar and SFD regions

Figure 3 shows a good agreement between the emission line strengths observed along and perpendicular to the bar for NGC 3185 and NGC 5970. This raises the question of

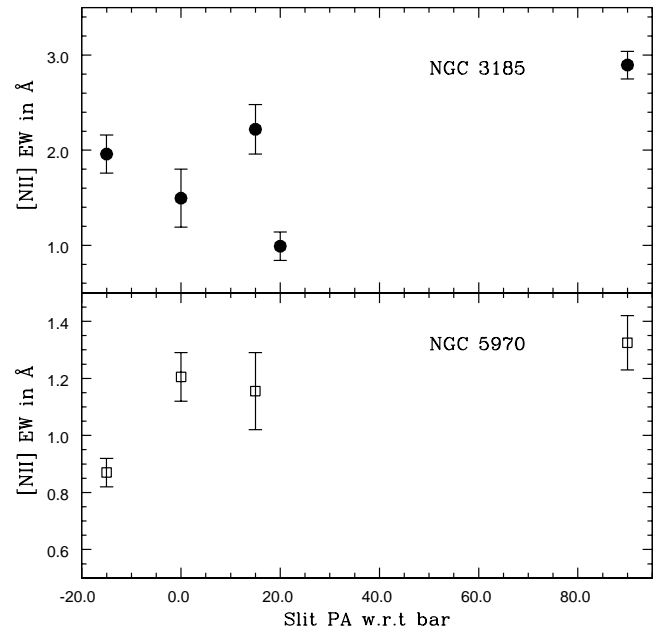


**Figure 3.**  $[NII]$  equivalent widths for multiple position angles relative to the bar axis. Solid circles show values for NGC 3185, and open squares the ratios for NGC 5970. Neither galaxy shows clear evidence for a systematic trend in spectral properties as a function of position angle.

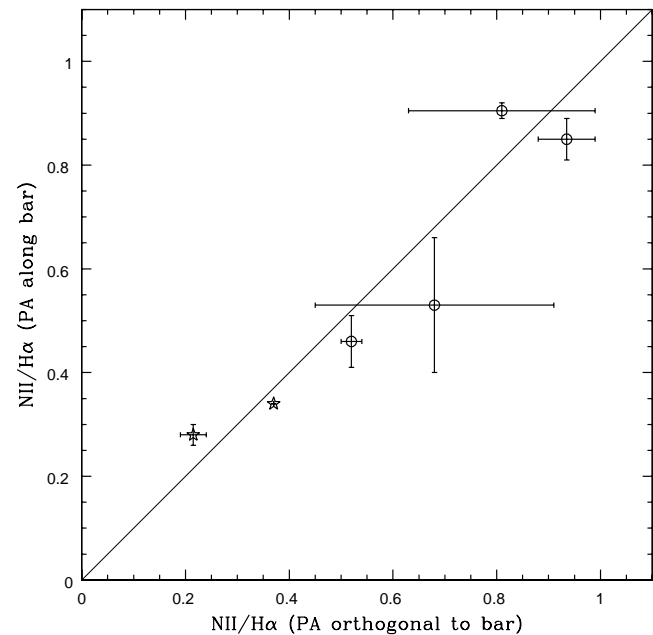


**Figure 4.**  $[NII]:H\alpha$  line ratios for regions lying along the bar (y-axis) vs. the same ratio extracted with the slit orientation orthogonal to the bar, within the same galaxies (x-axis), and covering the same radial ranges. The  $H\alpha$  fluxes have been corrected for the  $H\alpha$  absorption as described in Section 3.2.

whether the spectroscopic properties of bars and SFD regions are generally similar. Detailed analysis of this question will be left for a later paper, but we can attempt a preliminary analysis using spectroscopy for 6 galaxies in the present sample for which we have spectra observed along the bar axis, in addition to the SFD spectra. Figure 4 shows the mean  $[\text{NII}]/\text{H}\alpha$  ratios measured along the bars, plotted against the same ratios measured in the SFD regions perpendicular to the bar, for these 6 galaxies. The error bars indicate the ratios measured on opposite sides of the nucleus as previously, and the one-to-one relation is indicated by the diagonal line. In every case, the radial ranges of the spectral regions along and perpendicular to the bar are identical. The galaxies shown in this figure include two late-type, SBcd galaxies, NGC 2604 and NGC 4904, shown as stars in Fig. 4. The other four galaxies, plotted as circles are (reading from left to right on that figure) NGC 5970 (type SBc), NGC 5735 (SBbc), NGC 3185 (SBa) and NGC 2487 (SBc).

HII ratios, i.e. consistent with excitation by recently-formed stars, are found in the two Scd galaxies, NGC 2604 and NGC 4904, both along the bars and in the ‘SFD’ regions. Inspection of SDSS *gri* colour images (not shown) confirms this, as both galaxies show very blue colours in their bars and the surrounding SFD regions. The SFD regions show lower continuum surface brightness than the disc outside the bar-swept region, possibly indicating that the bars have started the removal of material from their surroundings, but the blue colours and emission lines with SF ratios confirm that this has not yet suppressed SF. As a consequence, it does not make sense to talk about SF ‘deserts’ in these galaxies, and this justifies the removal the 5 late-type Scd galaxies from the statistics discussed in Sect. 3.3.

For the 8 bar regions remaining after removal of the Scd-types, again after the application of absorption corrections, the mean observed  $[\text{NII}]/\text{H}\alpha$  ratio is  $0.686 \pm 0.080$ , median 0.729. A K-S test finds that these bar line ratios are completely consistent with being drawn from the same distribution as the ratios found in the SFD regions. However, it is highly unlikely that they are drawn from the same distribution as the ratios measured from HII regions. The bar and SFD line ratio statistics confirm the visual impression from Fig. 4 that the bars in at least this sub-sample contain stellar population with similar spectroscopic properties to their surrounding disc regions. However, this is a very small sample of galaxies and a very restricted set of properties, so we will return to this question in a later study.

### 3.6 Sulphur line ratios as a diagnostic of electron density.

At the referee’s suggestion, we have investigated whether we can derive useful constraints on ambient gas densities from our spectroscopic observations. Proxauf, Öttl & Kimeswenger (2014) present models of the emission line ratio  $[\text{SII}]6716\text{\AA}/[\text{SII}]6732\text{\AA}$  as a function of electron number density. These lines are detected at good signal-to-noise in most of our spectra. In Fig. 5, we present the resulting estimates of electron number density as a function of  $\text{H}\alpha$  EW. The points with the highest EW values, above  $7\text{\AA}$ , are predominantly late-type galaxies with SF-dominated line emission, as discussed previously (see Fig. 2). For the remaining population, dominated by

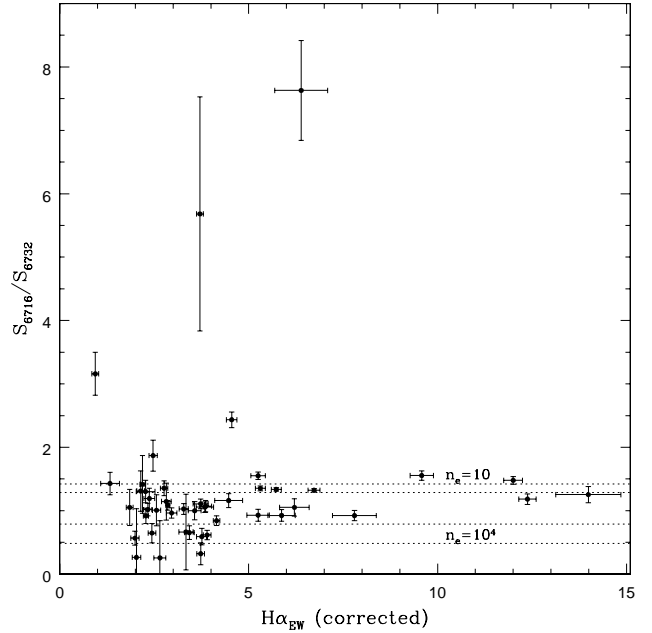


**Figure 5.** The emission line ratio  $[\text{SII}]6716\text{\AA}/[\text{SII}]6732\text{\AA}$  as a function of  $\text{H}\alpha$  equivalent width. The dotted horizontal lines correspond to the predicted ratios for electron densities of 10, 100, 1000 and 10,000  $\text{cm}^{-3}$  from top to bottom, respectively.

LINER-type emission, there is no evidence for a trend in line ratio, and hence  $n_e$ , with emission line strength. Most of the regions lie within the range  $100 < n_e < 1000$ , with outliers both above and below this range.

## 4 DISCUSSION

Several results emerge from this analysis of 48 barred galaxies. We confirm our earlier findings that strong bars have a profound effect on star formation in the central few kpc of galaxies. With the exception of the five SBcd galaxies, all of the galaxies studied show the SFD phenomenon, with no evidence of SF-driven emission line ratios in the regions swept by the bars of these 43 spiral galaxies. However, we also confirm the presence of diffuse line emission from almost all of these SFD regions, as first reported in James & Percival (2015). The smooth morphology of this emission is very different from the clumpy emission that characterises HII regions, and favours an association with the older stellar population that is present throughout these SFD regions. It extends several kpc from the galaxy centres, arguing against AGN as the powering mechanism.

This diffuse emission is close to ubiquitous, with  $[\text{NII}]$  line emission observed in 93 out of 101 SFD regions observed (92 per cent of SFD region spectra). The fraction with  $\text{H}\alpha$  line emission is at least as high with 96 regions showing emission, after correction for underlying  $\text{H}\alpha$  absorption. The distributions of  $[\text{NII}]/\text{H}\alpha$  line ratio (Fig. 1 lower frame),  $\text{H}\alpha$  EW (Fig. 2) and  $[\text{NII}]$  EW all show quite narrow distributions, with no obvious bimodality. This ubiquity and uniformity of spectroscopic properties favours p-AGB over EHB stars as the ionising source. While there are no direct

constraints on the presence or absence of EHB stars in the SFD regions, evidence from resolved populations in globular clusters (Catelan 2009; Torelli et al. 2019) shows that only about one-half of these systems have horizontal branches that extend to very blue colours. In a galactic context, the UV-upturn phenomenon, which is believed to be driven by EHB stars (Carter, Pass, Kennedy, Karick & Smith 2011), is found to vary greatly in strength from galaxy to galaxy, and is strongest in the centres of bright elliptical galaxies with high  $[\alpha/\text{Fe}]$  abundance ratios, a very different environment to the SFD regions of spiral galaxies. The uniformity of the line emission properties found here is much more easily explained if the emission is associated with p-AGB stars, which are themselves likely to be ubiquitous in intermediate-age and old stellar populations. Hence we take this as our working assumption for the rest of this discussion.

When we compare our observations of SFD regions with the p-AGB emission line models of Byler et al. (2017, 2019), some striking agreements are found, but there are also some interesting discrepancies. The  $[\text{NII}]/\text{H}\alpha$  line ratio distribution shown in the lower frame of Fig. 1 shows quite a tight clustering of values around a mean of 0.648. This is in excellent agreement with the ‘Fiducial’ model shown in fig. 8 of Byler et al. (2019), which predicts a logarithmic  $[\text{NII}]/\text{H}\alpha$  ratio of  $-0.2$ , or a ratio of 0.63, where the gas excited by the p-AGB stars has solar metallicity and abundance ratios. Byler et al. (2019) introduce a modified set of models, with enhanced abundances of  $\alpha$  elements, carbon and nitrogen (termed  $\alpha\text{CN}$  models) to simulate the effects of the local gas being dominated by gas ejected by the earlier evolution of the AGB stars themselves. They find that these  $\alpha\text{CN}$  models successfully reproduce the line ratios characteristic of the LINER/LIER region of the Baldwin, Phillips, & Terlevich (1981) and Kewley, Groves, Kauffmann & Heckman (2006) diagnostic diagrams, including  $[\text{NII}]/\text{H}\alpha$  ratios of approximately 2.0 – 3.0. However, our SFD spectra are clearly inconsistent with these  $\alpha\text{CN}$  model predictions, so we conclude that the observed  $[\text{NII}]/\text{H}\alpha$  line ratios are best explained by p-AGB stars ionising ambient interstellar medium, which must have sufficient density to dominate over AGB wind material. The presence of significant amounts of ambient gas may also explain why the line emission is marginally stronger ( $2 - 4 \text{ \AA}$  EW in  $\text{H}\alpha$ , see Fig. 2) compared with the model predictions ( $0.2 - 2.5 \text{ \AA}$ ). Unfortunately, our analysis of  $\text{SII}$  emission line ratios does not show any clear evidence for a dependence of the strength of this LINER-type emission on local gas density as traced by  $n_e$ . Further work on this question, particularly a comparison with stellar populations in passive early-type galaxies, would be instructive.

A controlling role for the gas supply in related contexts has been suggested previously. Graves et al. (2007), in an analysis of nuclear SDSS spectroscopy (and thus rather different environments from the present study), find LINER-type emission to be common but not ubiquitous in early-type galaxies. They conclude that significant ionising flux should be provided by p-AGB stars in all old stellar populations, and that this is the likely source powering such extended LINER emission; those galaxies without such emission are then explained through the absence of gas. Comparing with the WHAN diagnostic diagrams presented by Cid Fernandes et al. (2011), who again analyse nuclear SDSS spectra to discriminate emission powered by star

formation, AGN and hot evolved stars, we find that our SFD regions lie in a region that is clearly in the LINER regime, but that is relatively poorly populated by nuclear regions. Thus the SFD regions lie below the EW values expected for star formation or strong AGN, but higher than those found by Cid Fernandes et al. (2011) for red sequence ‘retired’ and passive galaxies. Again, this indicates that SFD regions have emission properties quite unlike those of least the central regions of any other galaxies, due to a combination of suppressed star formation, but higher ambient gas densities than are found in most quenched galaxies.

However, there is clear evidence, both from observations and simulations, that bars do deplete gas in SFD regions. In a study of simulations of strongly-barred spiral galaxies, Donohoe-Keyes et al. (2019) show significant removal of gas from SFD regions, suppressing star formation, within  $\sim 1$  Gyr of the formation of the bar. This finding is confirmed, for one galaxy at least, by the observational study of George et al. (2019), who present an analysis of the gas properties of the very nearby SBb galaxy NGC 3351, which was included in James & Percival (2015) and hence also in the present study. George et al. (2019) found that the SFD region, and most of the bar itself, are significantly depleted in both atomic and molecular gas, as traced by 21 cm radio and CO line emission respectively. Thus the bar appears to be funnelling gas from the entire region surrounding the bar into the nucleus of NGC 3351. However, in the present paper, we do find  $[\text{NII}]$  emission from the SFD region of this galaxy, and  $\text{H}\alpha$  emission after application of the  $\text{H}\alpha$  absorption correction. Thus there must be some gas present, as this line emission is clearly stronger than that from heavily gas-depleted passive galaxies (e.g. Cid Fernandes et al. 2011). In this context, it is interesting to note that the simulation-based study of Donohoe-Keyes et al. (2019) finds that, even after bars and SFD regions are fully established, significant radial migration occurs, bringing both stars and gas from the outer disc into the SFD regions. In the simulations, this radial flow does not re-establish star formation in the SFD regions, but it might be sufficient to explain the emission line properties found here.

DIG, excited by ionizing photons leaking from  $\text{HII}$  regions is likely to make at least some contribution to the diffuse extended emission discussed here. However, we feel that it is not the most natural explanation for the majority of this emission, over the full extent of these SFD regions. While Zurita et al. (2002) describe the DIG as an extended component, their models show it as still be generally concentrated around star-forming complexes as an extended halo (see e.g. their Fig. 4). In the SFD regions of the present study, the emission is smoothly distributed over the full extent of the regions, covering many kpc, with no evidence for any  $\text{HII}$  regions within the SFD regions. In addition, while Belfiore et al. (2016) find evidence in their IFU observations for LINER-like ratios from DIG emission, they also find that such emission is strongest close to regions of SF, and that the line ratios cluster on the borderline between LINER-like and SF excitation. Zhang et al. (2017) take this further, concluding, that ‘Leaky  $\text{HII}$  region models cannot produce LI(N)ER-like emission...LI(N)ER-like emission needs another ionization source’. Thus we focus in the present work on pAGB excitation as our preferred interpretation for the dominant excitation source in the regions observed in this

paper. However, there is an interesting debate to be had on the size and fraction of the contribution made by DIG, and we emphasise the importance of further observations of these SFD regions, where the extended scales may give unique insights into the DIG and pAGB contributions.

In summary, we find an important role for gas supply as a controlling factor in the observed properties of these SFD regions. While they are expected to be sufficiently gas-depleted so as to completely suppress star formation, the strength and line ratios of the diffuse line emission is most easily explained by p-AGB stars surrounded by significant amounts of ambient gas of approximately solar abundance. We note that there is support for this picture in the unusual properties of a post-merger barred galaxy, NGC 3729, described in Appendix A. Further study is required to determine why the gas in these SFD regions does not result in star formation.

## 5 CONCLUSIONS

The main conclusions of the present study are as follows:

- We confirm the SFD phenomenon of local suppression of star formation by bars, in the largest sample to date, 48 galaxies.
- The phenomenon occurs in virtually all early-type spirals (SBa - SBc), but 5 SBcd galaxies in the current sample retain star formation throughout their bars and surrounding regions.
- Diffuse H $\alpha$  and [NII] line emission is seen in almost all SFD regions, with [NII]/H $\alpha$  line ratios of 0.65 being typical, and EWs of 1.5 – 4 Å.
- The ubiquity and homogeneity of the line emission across all of the galaxies studied here argues for p-AGB stars, rather than e.g. EHB stars, as the dominant ionisation source.
- Line ratios are consistent with models of excitation of solar-abundance gas by p-AGB stars.
- The strength of the emission lines argues for a higher ambient gas density than is found in passive red-sequence galaxies.
- A preliminary comparison of the emission-line properties of bars and SFD regions finds little difference between the two environments within a given galaxy.
- Further study is needed to determine why the SFD region gas content identified here results in no detectable star formation.

In many ways, the SFD regions seem to represent a unique galactic environment, both in terms of their star formation properties, and in the emission lines resulting from their evolved stellar populations.

## ACKNOWLEDGMENTS

We thank the anonymous referee for several suggestions which significantly improved the paper. The Isaac Newton Telescope is operated on the island of La Palma by the Isaac Newton Group in the Spanish Observatorio del Roque de los Muchachos of the Instituto de Astrofísica de Canarias.

This research has made use of the NASA/IPAC Extragalactic Database (NED) which is operated by the Jet Propulsion Laboratory, California Institute of Technology, under contract with the National Aeronautics and Space Administration. This research has made use of the NASA/IPAC Extragalactic Database (NED) which is operated by the Jet Propulsion Laboratory, California Institute of Technology, under contract with the National Aeronautics and Space Administration. Funding for the SDSS and SDSS-II has been provided by the Alfred P. Sloan Foundation, the Participating Institutions, the National Science Foundation, the U.S. Department of Energy, the National Aeronautics and Space Administration, the Japanese Monbukagakusho, the Max Planck Society, and the Higher Education Funding Council for England. The SDSS Web Site is <http://www.sdss.org/>. The SDSS is managed by the Astrophysical Research Consortium for the Participating Institutions. The Participating Institutions are the American Museum of Natural History, Astrophysical Institute Potsdam, University of Basel, University of Cambridge, Case Western Reserve University, University of Chicago, Drexel University, Fermilab, the Institute for Advanced Study, the Japan Participation Group, Johns Hopkins University, the Joint Institute for Nuclear Astrophysics, the Kavli Institute for Particle Astrophysics and Cosmology, the Korean Scientist Group, the Chinese Academy of Sciences (LAMOST), Los Alamos National Laboratory, the Max-Planck-Institute for Astronomy (MPIA), the Max-Planck-Institute for Astrophysics (MPA), New Mexico State University, Ohio State University, University of Pittsburgh, University of Portsmouth, Princeton University, the United States Naval Observatory, and the University of Washington.

## REFERENCES

- Allen M. G., Groves B. A., Dopita M. A., Sutherland R. S., Kewley L. J., 2008, *ApJS*, 178, 20
- Baldwin J. A., Phillips M. M., Terlevich R., 1981, *PASP*, 93, 5
- Belfiore F. et al., 2016, *MNRAS*, 461, 3111
- Binette L., Magris C. G., Stasińska G., Bruzual A. G., 1994, *A&A*, 292, 13
- Bremer M., Scharwächter J., Eckart A., Valencia-S. M., Zuther J., Combes F., Garcia-Burillo S., Fischer S., 2013, *A&A*, 558, A34
- Brocklehurst M., 1971, *MNRAS*, 153, 471
- Byler N., Dalcanton J. J., Conroy C., Johnson B. D., 2017, *ApJ*, 840, 44
- Byler N., Dalcanton J. J., Conroy C., Johnson B. D., Choi J., Dotter A., Rosenfield P., 2019, *arXiv*, arXiv:1904.10978
- Caldwell N., 1984, *PASP*, 96, 287
- Carter D., Pass S., Kennedy J., Karick A. M., Smith R. J., 2011, *MNRAS*, 414, 3410
- Catelan M., 2009, *Ap&SS*, 320, 261
- Choi J., Dotter A., Conroy C., Cantiello M., Paxton B., Johnson B. D., 2016, *ApJ*, 823, 102
- Cid Fernandes R., Stasińska G., Mateus A., Vale Asari N., 2011, *MNRAS*, 413, 1687
- den Brok M., et al., 2020, *MNRAS*, 491, 4089
- Donohoe-Keyes C. E., Martig M., James P. A., Kraljic K., 2019, *MNRAS*, 489, 4992

- Dotter A., 2016, *ApJS*, 222, 8  
 Ferguson A. M. N., Wyse R. F. G., Gallagher J. S., Hunter D. A., 1996, *AJ*, 111, 2265  
 Ferland G. J., et al., 2013, *RMxAA*, 49, 137  
 Friedli D., Benz W., 1993, *A&A*, 268, 65  
 George K., Joseph P., Mondal C., Subramanian S., Subramanian A., Paul K. T., 2019, *A&A*, 621, L4  
 Gomes J. M., et al., 2016, *A&A*, 588, A68  
 Goudfrooij P., 1999, in Carral P., Cepa J., eds, *Star Formation in Early-type Galaxies*, ASP Conf. Ser. Vol. 163. Astronomical Society of the Pacific, p. 55  
 Graves G. J., Faber S. M., Schiavon R. P., Yan R., 2007, *ApJ*, 671, 243  
 Haffner L. M., et al., 2009, *RvMP*, 81, 969  
 Hakobyan A. A., et al., 2014, *MNRAS*, 444, 2428  
 Hirschmann M., Charlot S., Feltre A., Naab T., Choi E., Ostriker J. P., Somerville R. S., 2017, *MNRAS*, 472, 2468  
 Hummer D. G., Storey P. J., 1987, *MNRAS*, 224, 801  
 James, P. A. et al., 2004, *A&A*, 414, 23  
 James P. A., Bretherton C. F. & Knapen J. H., 2009, *A&A*, 501, 207  
 James P. A., Percival S. M., 2015, *MNRAS*, 450, 3503  
 James P. A., Percival S. M., 2016, *MNRAS*, 457, 917  
 James P. A., Percival S. M., 2018, *MNRAS*, 474, 3101  
 Kewley L. J., Groves B., Kauffmann G., Heckman T., 2006, *MNRAS*, 372, 961  
 Kormendy J., & Kennicutt R. C., 2004, *ARAA*, 42, 603  
 Kormendy J., 2013, in Falcon-Barroso J., Knapen J. H., eds, *Secular Evolution of Galaxies*, XXIII Canary Islands Winter School of Astrophysics, Cambridge University Press, Cambridge, p. 1  
 Nair P. B., Abraham R. G., 2010, *ApJ*, 714, L260  
 Papaderos P., et al., 2013, *A&A*, 555, L1  
 Percival S. M., Salaris M., Cassisi S. & Pietrinferni A., 2009, *ApJ*, 690, 427  
 Phillips M. M., Jenkins C. R., Dopita M. A., Sadler E. M., Binette L., 1986, *AJ*, 91, 1062  
 Proxauf B., Öttl S., Kimeswenger S., 2014, *A&A*, 561, A10  
 Singh R., et al., 2013, *A&A*, 558, AA43  
 Stasińska G., et al., 2008, *MNRAS*, 391, L29  
 Torelli M., et al., 2019, arXiv, arXiv:1907.09568  
 Weilbacher P. M., et al., 2018, *A&A*, 611, A95  
 Zhang K., et al., 2017, *MNRAS*, 466, 3217  
 Zurita A., Beckman J. E., Rozas M., Ryder S., 2002, *A&A*, 386, 801

## APPENDIX A: AN UNUSUAL MERGING BARRED GALAXY NGC 3729

In this Appendix, we describe a somewhat unusual barred galaxy, NGC 3729. This has a classification of SBa (pec), with the peculiar nature being linked to a probable late-stage minor merger, as illustrated in the SDSS colour composite image in Fig. A1. The low-surface-brightness feature to the north-east of NGC 3729 may be the tidally-shredded remains of a low-mass companion, and the mottled appearance of the upper half of NGC 3729 may be due to dusty gas accreted during this interaction. We adopt a distance of 20.2 Mpc for this system.

Spectroscopically, NGC 3729 shows strong and complex central emission, and emission from a bar-end ring, all of



**Figure A1.** SDSS colour composite image on NGC 3729. Note the low surface brightness component to the north-east, which may indicate an ongoing minor merger.

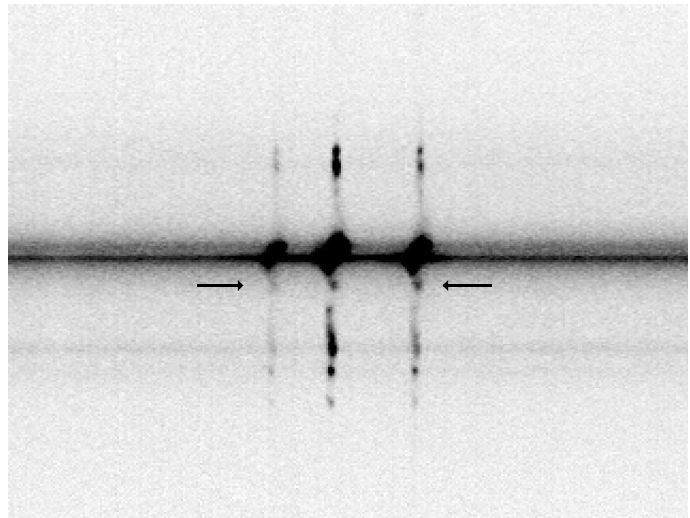


**Figure A2.** Two-dimensional optical spectrum of NGC 3729, centred on the  $H\alpha$  and  $[\text{NII}]$  lines. The emission-line clump is indicated by the arrows. Comparison with the bright  $\text{HII}$  region towards the bottom of the frame shows the extended nature of the line emission from the clump.

which has  $[\text{NII}]/H\alpha$  ratios fully consistent with star formation; see the 2-dimensional spectrum in Fig. A2, taken with the INT and IDS at a slit position angle of  $290^\circ$ , perpendicular to the bar. The bar-end ring results in the strong peaks of emission towards the top and bottom of this figure, at distance of  $19''$  or 1.8 kpc from the nucleus. The spectrum shows complex nuclear structure, with multiple components, including a very rapidly rotating structure, which we inter-

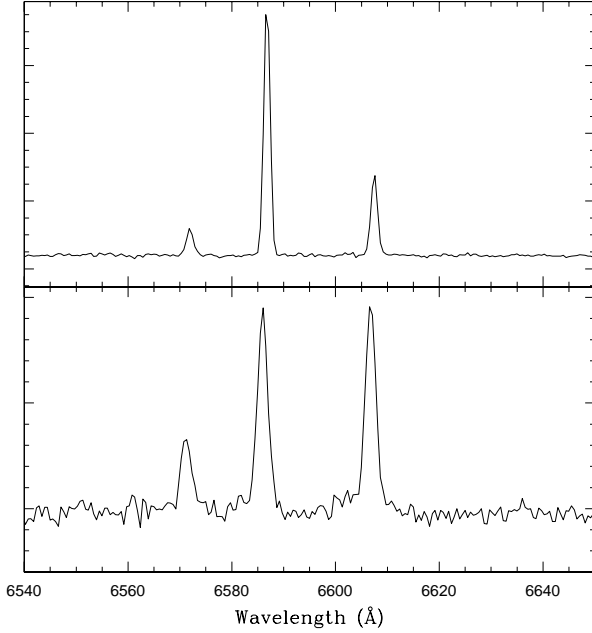


**Figure A3.** Extracted  $H\alpha$  and  $[\text{NII}]$  emission for the NGC 3729 clump (bottom) and, for comparison, an HII region in the same galaxy (top). The high  $[\text{NII}]/H\alpha$  ratio in the clump is clearly apparent.

pret as a star-forming nuclear ring. Between the nuclear and bar-end rings, diffuse emission is apparent, particularly in the upper part of Fig. A2. Thus, in spite of its peculiarity, we do consider this an example of the SFD phenomenon, and it is included as such in the present paper.

The unusual feature seen in Fig. A2 is the peak of emission seen just below the nuclear ring,  $5.7''$  (560 pc) from the nucleus. At first sight, this resembles an HII region, but uniquely, in the current data set at least, it shows clear LINER-type ratios. To illustrate this point, Fig. A3 shows the extracted spectrum of this peak in the lower frame, with an HII region spectrum from the same long-slit observation shown in the upper frame for comparison. The spectra are clearly different, and argue against ongoing star formation in the near-nuclear clump. The clump has  $[\text{NII}]$  and  $H\alpha$  EW values of 5.63 and 6.73 Å respectively, similar to or slightly greater than the values for the two SFD regions in NGC 3729 (4.70 and 3.69 Å for  $[\text{NII}]$ , 6.76 and 4.50 Å for  $H\alpha$ ). These values are all at the high end of the EW distributions for line emission from SFD regions, while the  $[\text{NII}]/H\alpha$  ratio for the clump, 0.837, is entirely consistent with the distribution of ratios for SFD regions (Fig. 1 lower panel).

One possibility is that the near-nuclear clump could be the nucleus of the tidally-shredded companion, that has been drawn towards the centre of NGC 3729 through dynamical friction. One test of this is to look for spatial extent. Visual inspection of Fig. A2 indicates that the clump appears moderately extended, e.g. compared with the most compact HII region (towards the bottom of the image). Measurements confirm this; along the spatial direction, the clump has a full-width at half maximum (FWHM) of 5.3 pixels, or  $2.33''$ , compared to 3.7 pixels or  $1.63''$  for the compact HII region.

As the latter may itself be somewhat extended, we also measured the FWHM of the standard star observation taken closest in time to the NGC 3729 spectra, finding values of 3.2 pixels or  $1.4''$ . Taking either the star or (conservatively) the HII region as a measure of the seeing broadening the clump FWHM, the true size of the clump is 1.9 or  $1.7''$  respectively. Taking the distance to the galaxy as 20.2 Mpc, the FWHM size of the clump is 163 - 182 pc, much larger than a stellar cluster. Thus this may be the extended central regions of a dwarf galaxy. We also note that the clump velocity is somewhat different from that of the disc and nuclear emission to either side of it, as might be expected if the clump were part of an interacting or merging system.

We note that NGC 3729 may well be an unusually gas-rich galaxy within the current sample, due to the merging activity, and evidenced by the clumpy absorption seen over much of the galaxy. This may explain the stronger-than-average line emission seen in the SFD regions of this galaxy. The gas would be expected to concentrate in the central regions of the galaxy, explaining the particularly high EW lines from the near-nuclear clump. Overall, the spectroscopic properties of the clump in NGC 3729 support the interpretation of diffuse line emission presented in this paper, with a ubiquitous source of ionising photons from old stellar populations in all locations, and the EW of the resulting line emission being controlled primarily by the gas supply. The line ratios in the clump are consistent with theoretical predictions where ambient gas of approximately solar abundance is dominant, as was found for the SFD regions in the present study.